ACS APPLIED MATERIALS & INTERFACES

www.acsami.org

Research Article

Rapid Size-Based Isolation of Extracellular Vesicles by Three-Dimensional Carbon Nanotube Arrays

Yin-Ting Yeh, Yijing Zhou, Donghua Zou, He Liu, Haiyang Yu, Huaguang Lu, Venkataraman Swaminathan, Yingwei Mao,* and Mauricio Terrones*

Cite This: *ACS Appl. Mater. Interfaces* 2020, 12, 13134–13139

Read Online

ACCESS | Metrics & More | Article Recommendations | Supporting Information

ABSTRACT: Recent discoveries reveal that extracellular vesicles (EVs) play an important role in transmitting signals. Although this emerging transcellular pathway enables a better understanding of neural communication, the lack of techniques for effectively isolating EVs impedes their studies. Herein, we report an emergent high-throughput platform consisting of three-dimensional carbon nanotube arrays that rapidly capture different EVs based on their sizes, without any labels. More importantly, this label-free capture maintains the integrity of the EVs when they are excreted from a host cell, thus allowing comprehensive downstream analyses using conventional approaches. To study neural communication, we developed a stamping technique to construct a gradient of nanotube herringbone arrays and integrated them into a microdevice that allowed us processing of a wide range of sample volumes, microliters to milliliters, in several minutes through a syringe via manual hand pushing and without any sample preparation. This microdevice successfully captured and separated EVs excreted from glial cells into subgroups according to their sizes. During capture, this technology preserved the structural integrity and originality of the EVs that enabled us to monitor and follow internalization of EVs of different sizes by neurons and cells. As a proof of concept, our results showed that smaller EVs (~80 nm in diameter) have a higher uptake efficiency compared to larger EVs (~300 nm in diameter). In addition, after being internalized, small EVs could enter endoplasmic reticulum and Golgi but not the largest ones. Our platform significantly shortens sample preparation, allows the profiling of the different EVs based on their size, and facilitates the understanding of extracellular communication. Thus, it leads to early diagnostics and the development of novel therapeutics for neurological diseases.

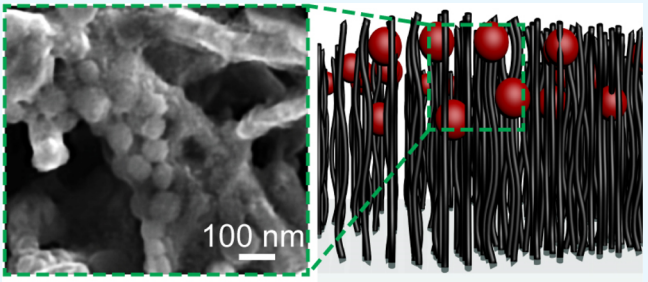

KEYWORDS: *extracellular vesicles, aligned carbon nanotube, size-based capture, cellular uptake, microdevice*

INTRODUCTION

Extracellular vesicles (EVs) are membrane-enclosed vesicles secreted by various types of cells, and they can freely circulate in the extracellular environment.[1] Based on their size, origin, and cargo content, EVs can be divided into three groups: exosome (30−100 nm in diameter), microvesicles (100 nm to 1 μm in diameter), and apoptotic bodies (0.8−5 μm in diameter).[2,3] The membrane of EVs is usually similar to the membrane of their originated organelles, which consists of the lipid bilayer and proteins, including membrane organizers, trafficking and adhesion proteins, and cell-specific proteins.[4] The cargo contents of EVs include proteins, lipids, and genetic materials, such as mRNAs, micro-RNAs (miRNAs), and noncoding RNAs.[1] By delivering and exchanging biological materials, EVs regulate the physiological conditions of the recipient cells.[5−7] EVs carry information and reflect the status of the cells when excreted, which may reveal the progress of specific diseases. Many studies have indicated that EVs may serve as the biomarkers in cancer,[8] infectious diseases,[9] neurological diseases,[10] and others.[11,12] For example, in a mammalian brain, EVs transfer reciprocal signals between glia and neurons, such as immune responses,[13] and synapse assembly.[14,15] Furthermore, in neurodegeneration diseases, EVs participate in the spreading of protein aggregates in Alzheimer's and Parkinson's diseases.[14,16,17] In brain tumors, cancer cells also upregulate excretions of EVs.[18] The released EVs involved in tumorigenic activity contain tumor-specific cargo compositions when compared to healthy cells.[8,9,18] In multiple sclerosis, a demyelinating disease,[19] EVs play an active role in spreading proinflammatory signals. The nervous system uses EVs as intercellular communication cargos, whether the host is healthy or ill. Therefore, the rapid capture of different

Received: November 22, 2019
Accepted: February 19, 2020
Published: February 19, 2020

https://dx.doi.org/10.1021/acsami.9b20990
ACS Appl. Mater. Interfaces 2020, 12, 13134−13139

EVs can promote early diagnosis and close monitoring of disease progression during treatment.[13,18,20,21]

EVs circulate in various types of body fluids, for example, blood, urine, saliva, and cerebrospinal fluid. Purifying EVs is the key to establish a comprehensive analysis. EVs consist of a heterogeneous mixture of particles at the submicrometer scale. Conventional approaches to enrich and isolate EVs include chemical capture, such as immunoaffinity-based capture, and density-based enrichments, such as ultracentrifugation. The immuno-based capture relies on the specific antigens present on the EV surface to be known. Unfortunately, these specific markers of the EVs are largely unavailable because of the current limited understanding of EVs.[18,22] Ultracentrifugation enriches different EVs based on their densities and sizes.[18,23] Unfortunately, this process takes hours or days, and studies have shown that intense centrifugal forces induce EV's deterioration, which impedes downstream analysis.[23] Therefore, and in order to preserve the sensitive cargo content of EVs, a faster, more efficient, and gentler isolation method than the currently available methods is urgently needed.[18,23−25]

In this paper, we present a label-free approach that rapidly isolates EVs of different sizes. We have developed and built a portable microdevice integrating aligned nitrogen-doped carbon nanotubes (CNxCNTs) forming three-dimensional (3D) arrays. We demonstrated that these 3D arrays are able to capture different EVs excreted from neurons within several minutes and without any sample preparation. Furthermore, this gentle and effective size-based capture process enabled us to study neural communication on-chip. For example, we tracked the uptake of the EVs of different sizes in real-time and discovered that they were internalized into different compartments of cells. Our results demonstrate that this label-free and rapid isolation platform could accelerate the discovery of EVs, thus providing relevant insights into cellular communications with impact in the early detection of different diseases.

CONCLUSIONS

Multiwalled carbon nanotubes (MWCNTs) consist of nested cylindrical nanostructures made of sp^2-hybridized carbon atoms.[26] CNTs possess unique properties and have been utilized in different applications, including electronics, optics, and functional nanotechnologies.[27,28] Beyond pristine MWCNTs, our previous studies have shown that N-doped MWCNTs (CNxCNTs) possess different electrical conductivity and enhanced biocompatibility when compared to pure carbon MWCNTs.[29−34] Accordingly, we used aligned CNxCNTs as the building block of our microdevices (Figures 1 and S1). In particular, we developed a microstamping technique to deposit Fe-containing precursors on SiO_2/Si substrates (Figure S2).[35] The microstamping technique allowed us to precisely pattern and grow aligned CNxCNT arrays, in a herringbone pattern, with a submillimeter resolution in a simple and cost-effective way, when compared to lithography-based techniques.[36] Previous studies have shown that fluidic microvortices induced by the herringbone patterns could enhance the mixing of the media circulating inside a microfluidic channel.[37,38] This stamping method allowed us to pattern Fe catalytic particles with a concentration gradient in a simple and low-cost process, when compared to a conventional lithography-based fabrication technique that involves a variety of chemicals and photoresists, several steps of patterning, including lithography and deposition, and that which has to be repeated sequentially. We constructed

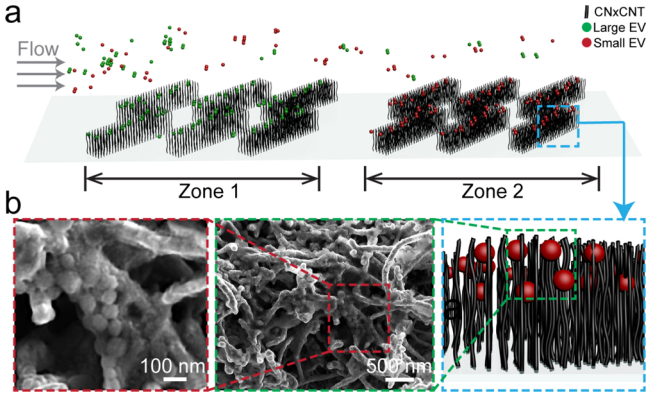

Figure 1. Aligned carbon nanotube arrays for size-based exosome capture. (a) Illustration of the size-based capture by different ITD zones of the CNxCNT arrays. (b) SEM images of the aligned CNxCNT arrays after capture.

herringbone arrays by aligned CNxCNTs with tunable intertubular distances (ITDs) ranging from 22 ± 5 to 720 ± 64 nm (Figure S3). The stamping process patterned multiple zones of the herringbone arrays with different ITDs to match a variety of EVs of different sizes.

This microdevice is designed to rapidly capture and separate different EVs according to their sizes, and it is also used to observe cellular uptake of the different trapped EVs. To ensure these characteristics, aligned CNxCNTs with ∼60 μm in height and having 80 and 300 nm ITDs captured and separated EVs into two subgroups (Figure 1a,b). Without any sample preparation, the CNxCNT-based herringbone microdevice successfully captured and separated EVs excreted from glia cells into two subgroups, ∼80 and ∼300 nm, by hand-pushing samples through a syringe (Figure S3a). After EV capture, we cultured different neural cells on the CNxCNTs containing the EVs and tracked the internalization of the different EVs.

We first used different sizes of fluorescently labeled particles to characterize the size-based capture of the constructed devices (Figure S4a). These spherical particles had uniform diameters. We estimated capture efficiencies by comparing the fluorescent intensities of the flow through to that of the original samples (Figure S4b). In order to characterize the size-based capture, first, we introduced particles of one size into the microdevice with one ITD (20, 100, 220, or 550 nm) under a flow rate of 200 μL/min. Each condition was repeated five times (N = 5). As shown in Figure 2a, when the size of the particles matches the ITD, the microdevices have a high capture efficiency. Next, we prepared mixtures of particles of different sizes (400, 140, and 25 nm in diameter) and loaded them into a microdevice consisting of nanotube zones with ITDs matching the different sizes of the particles (Figure S5a). After capture, strong fluorescent signals of an individual subgroup of particles were detected in the respective zones, comprising the CNxCNT arrays with ITDs matching the sizes of the particles. As shown in Figure S5b, fluorescent images clearly revealed that different particles were captured and separated according to their sizes. The capture efficiency of particles with diameters of 400, 140, or 25 nm could reach 31.8 ± 3.3, 34.3 ± 4.5, or 35.3 ± 4.7%, respectively, when the flow rate varied from 250 to 500 μL/min (Figure S6a,b). In this flow rate range, the herringbone array could effectively enhance the mixing of the samples.[38] We assembled microdevices without CNxCNTs to further confirm that the

https://dx.doi.org/10.1021/acsami.9b20990
ACS Appl. Mater. Interfaces 2020, 12, 13134−13139

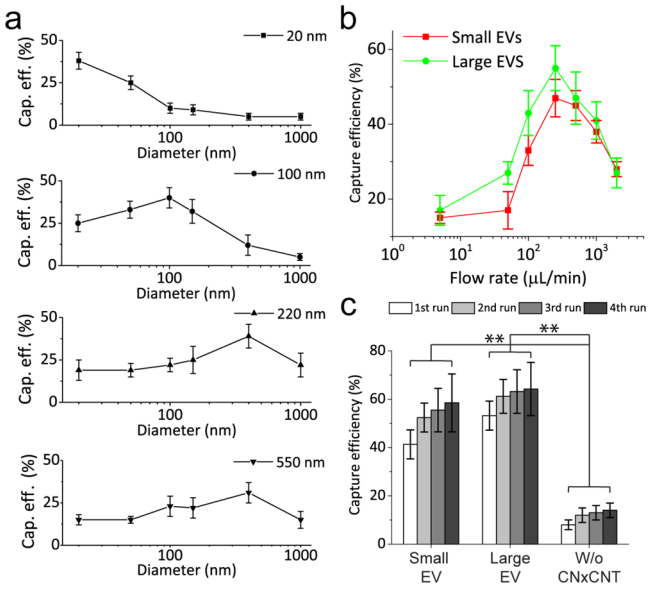

Figure 2. Characterization of the size-based capture (N = 5). (a) Capture efficiencies of particles of different diameters by microdevices with different ITDs. (b) Capture efficiencies of the different sizes of the mixed EVs by microdevice with ITDs of 300 and 100 nm. (c) Capture efficiencies of the microdevices after repeating the process of the capture. $p < 0.01$.

CNxCNT arrays promoted the size-based capture. After loading the same mixture of the particles (400, 140, and 25 nm in diameter), we measured the capture efficiency to be less than 8%, which was contributed by nonspecific capture (Figure S6c,d). The results confirmed that the CNxCNT arrays are effective in capturing particles according to their sizes.

EVs consist of a heterogeneous mixture of vesicles and can be categorized into subgroups based on their size, composition, and origin.[18] Recent studies have demonstrated that EVs play a key role in neurodegeneration disease[39] and brain development[40] and can facilitate new ways of neural communication.[41] In this context, a novel method for label-free and size-based capture would result in a new approach to study the role of different EVs. As a proof of concept, we fabricated microdevices with ITDs of 300 nm (zone 1) and 80 nm (zone 2) to separate EVs excreted from cultured mouse primary glial cells by hand pushing through a syringe. As observed under scanning electron microscopy (SEM), the EV-like particles are captured and embedded in between the aligned CNxCNTs (Figure 1b). We then applied western blotting to detect protein expressions of the captured EV-like particles. The results confirmed that EVs were successfully captured according to their size (Figure S7). By fluorescence labeling of EVs and after recording the fluorescent intensities before and after capture, the capture efficiencies of the EVs were systematically determined (Figure S8). After capture, strong fluorescent signals were detected in both zones, and the wavelength of the fluorescence indicated that the microdevice successfully separated the EVs, according to their sizes, with capture efficiencies of 47.5 ± 5.1 and 55.4 ± 4.2% for small and large EVs, respectively (Figures 2b, S9, and S10). Noticeably, the capture efficiencies are higher when the flow rate ranges between 100 and 500 μL/min. We believe that under this range, the microvortices caused by the herringbone arrays promote the mixing of the samples, thus enhancing the interaction between the EVs and the 3D CNxCNT arrays. We also examined whether repeating the capture would enhance the capture efficiencies and as shown in Figure 2c; no statistically significant improvement was noted up to four repeats. As noted above, the nonspecific capture efficiencies of the EVs by the microdevices without CNxCNT arrays was ~20% (Figure S10), more than a factor of 2 less than that of the microdevices with the CNxCNTs, thus confirming once again the role of the CNxCNT arrays in the efficient size-based capture.

After capturing EVs, we then cultured primary glial cells and neuroblastoma (SH-SY5Y and ATCC-2266) on the aligned CNxCNT arrays and observed the uptake of EVs in real time (Figure 3). A standard cell culture procedure, as instructed by

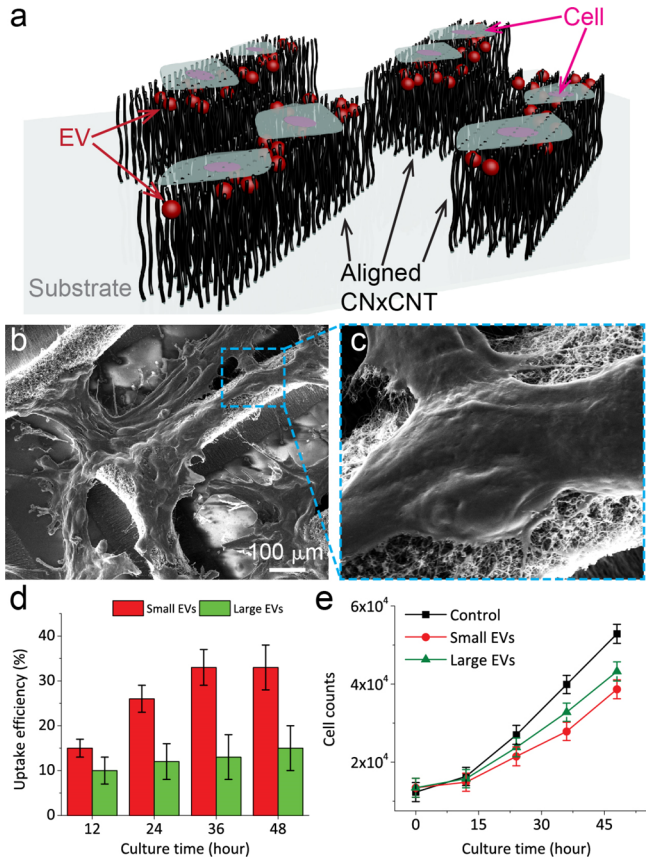

Figure 3. On-chip uptake of the captured EVs. (a) Illustration of the cell culture on-chip for the EV uptake study. (b,c) SEM images of SY5Y cell culture on aligned CNxCNT arrays with embedded EVs. (d) Uptake efficiency of the captured EVs. (e) Doubling time of SY5Y after uptake of the different EVs.

the manufacture, was followed.[42] It was noted in the SEM images that both cells attach and proliferate on the CNxCNT arrays (Figures 3b,c and S11). During cell culture, cells move to the CNT arrays, thus helping the release of EVs for intake. More importantly, fluorescence signals were detected inside cells with wavelengths associated with the previously labeled EVs (Figure S12). We estimated an uptake efficiency, defined as the ratio of the number of cells with fluorescent signals, and the total number of cells across the CNxCNT arrays. In general, small EVs have a higher uptake efficiency than the larger ones (Figure 3d), which is consistent with previous suggestions that smaller particles tend to be internalized by cells.[43] For smaller EVs, their uptake efficiencies increased

https://dx.doi.org/10.1021/acsami.9b20990
ACS Appl. Mater. Interfaces 2020, 12, 13134−13139

during the culture over time and then reached a plateau after 36 h when the cells reached ~100% confluency. For large EVs, the uptake efficiencies did not show any appreciable change over culture time. To further evaluate the viability of the cells after the EV uptake, we transferred the cells back to the culture plates and monitored their proliferation by measuring their doubling time. Both cells were proliferated over 48 h and compared to cells without internalizing EVs, as a control experiment (Figures 3e and S13). Cells internalized with EVs were proliferated. However, the doubling time is slower than the control, especially for those internalized with the smaller EVs. The results suggest that EVs excreted from the glial cells slow down the doubling time of SY5Y cells after internalization. Furthermore, because small EVs tend to be more internalized by the cells than the larger ones, they also had a slower doubling time than that of the larger EVs.

We applied confocal microscopy to track the uptake of EVs inside the cells (Figure 4). The *z*-stack scanning of the

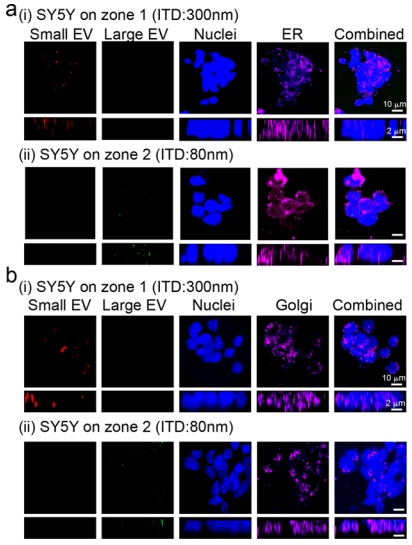

Figure 4. Confocal microscopy images of SY5Y cells after uptake of smaller (red) and larger (green) EVs. The upper rows of each image set are top-view images, and the lower rows of each image set are cross-sectional images. (a) Staining of small EV (red), large EV (green), nuclei (blue), ER (pink), and combined images. (b) Staining of small EV (red), large EV (green), nuclei (blue), Golgi (pink), and combined images.

fluorescent signals showed that both small and large EVs were detected inside the cells. Thus, it was again confirmed that cells internalized more small EVs than the large ones. By overlapping the fluorescent signals from the endoplasmic reticulum (ER) and Golgi (Figure 4a,b), small EVs (shown in red) were detected in both ER and Golgi compartments. In contrast, while large EVs (shown in green) were internalized by the cells, they neither enter the ER nor the Golgi compartments. This observation is consistent with studies showing that exosomes transport through endocytic vesicles after uptake and interact with the ER before being secreted into the lysosome.[44−46]

In conclusion, we have developed an effective stamping technique to grow arrays of aligned CNxCNTs to fabricate microfluidic devices that successfully captured and separated different EVs according to their sizes without any labels or sample preparation. With this novel technology, we have demonstrated the feasibility of studying the effect of size within EVs and tracked their internalization in living neuronal cells. This technological platform enables a new approach for the discovery and rapid profiling of different EVs in order to gain key insights into cellular communication.

METHODS

Stamping Technique for CNxCNT Growth. A mold with a pattern for stamping was designed by Solidwork (v2018) and manufactured by a 3D printer (FlashForge Creator Pro) with polylactide. Subsequently, we applied polydimethylsiloxane (PDMS) to coat the molds and cure overnight for cross-linking. Precursor solutions were prepared by diluting $Fe(NO_3)_3{\cdot}9H_2O$ (Sigma-Aldrich, #254223-10G) using a mixture (1:1) of deionized (DI) water and toluene (Sigma-Aldrich, #244511-100ML). To start stamping, 50 μL of the precursor solution was spun on a silicon substrate (1 cm by 1 cm) with a 300 nm thick oxide layer under 100 rpm for 5 s, followed by 500 rpm for 20 s. Prior to microcontact printing, both PDMS-coated stamps and glass substrates were treated by a light air plasma. To perform microcontact printing, a PDMS stamp was placed on a silicon substrate coated with iron precursors for 30 s. Then, the PDMS stamp was applied on a glass substrate for 1 h in order to ensure that the iron precursors were transferred to the substrate and dried.

Growth of the CNxCNT. The growth was performed by chemical vapor deposition (CVD). In particular, benzylamine (Fluka, CAS: 100-46-9) was fed through the system by a nebulizer, working as both carbon source and nitrogen dopant. The furnace temperature ramped to 825 °C in 30 min. When the temperature reached 825 °C, we turned on the nebulizer and increased the argon and 15% hydrogen flow to 2.5 L/min. After growth, image analysis was performed using field emission SEM (LEO 1530 FESEM) to measure the dimensions through cross-sectional images.

Capture Efficiency Measurement. Fluorescently labeled particles were purchased from Thermo Fisher Scientific and diluted by DI water. Fluorescent intensity was measured by a microplate reader (Tecan Infinite F200). The capture efficiency was calculated by measuring and comparing the fluorescent intensities before and after the captures.

Raman Spectra Measurements of CNxCNT. We used Raman microscopy (Renishaw, InVia Raman microscopy) to characterize the AACVD-synthesized CNxCNTs. In particular, the CNxCNT sample was synthesized for 30 min using the procedure as described. We recorded the Raman spectra using 514 nm laser excitation for 30 s under 50× magnification. The laser power to the sample was 10 μW.

Sample Preparation for Electron Microscopy. For SEM sample preparation, the samples were fixed with 4% paraformaldehyde and were then dehydrated with ethanol under a serial dilution from 50 to 100% (pure ethanol). For TEM, the samples were dropped onto Quantifoil Copper grids treated with a mild air plasma (PELCO easiGlow Glow Discharge Cleaning System) and then negative staining was applied.

Cell Culture. The human glioblastoma astrocytoma cell line U-251 MG, the human neuroblastoma cell line SY5Y, and the LMH cell line (ATCC CRL-2117) were cultured in high-glucose Dulbecco's Modified Eagle's Medium supplemented with 10% fetal bovine serum (FBS), 100 units/mL penicillin, and 100 μg/mL streptomycin (Invitrogen) in a cell culture incubator at 5% CO_2 and 37 °C ambient temperature. FBS was removed from the culture media 12 h before EV collection. Cells were cultured to 70−90% confluency and then lifted with 0.05% trypsin−ethylenediaminetetraacetate (Invitrogen).

Immunofluorescence Staining. Cells were scraped from the device, seeded on the coverslips in the culture media, and fixed in 4% paraformaldehyde. Before staining, the coverslips were rinsed with phosphate-buffered saline (PBS) three times and then blocked in 5% donkey serum diluted in Tris-buffered saline with 0.1% Tween for 1 h. Primary antibodies were diluted in the blocking media. Anti-calnexin antibody (Santa Cruz, sc-23954, used 1:1000) was used to label ER,

https://dx.doi.org/10.1021/acsami.9b20990
ACS Appl. Mater. Interfaces 2020, 12, 13134−13139

and anti-GM130 antibody (BD Transduction Laboratories, 610882, used 1:1000) was used to label the Golgi apparatus. After overnight blocking in the primary antibody and rinsing thrice in PBS, the secondary antibody (Thermo Fisher, A32787) diluted in the blocking media was applied for 1 h. The coverslips were then rinsed three times with PBS, incubated with DAPI, and mounted in ProLong Gold (Thermo Fisher, P10144). The whole process was performed in room temperature.

■ ASSOCIATED CONTENT

Supporting Information

The Supporting Information is available free of charge at https://pubs.acs.org/doi/10.1021/acsami.9b20990.

> Material characterization of CNxCNTs; design and assembly of the microdevice; tunable dimensions of the CNxCNT arrays; characterization of the fluorescently labeled particles; characterization of the size-based capture; characterization of the capture efficiency; results of western blotting; preparations of different size EVs; fluorescent and optical images of a microdevice; capture efficiency of the EVs; SEM image of glia culturing; fluorescent images of label-free EV capture and uptake; and doubling time of glia culturing (PDF)

■ AUTHOR INFORMATION

Corresponding Authors

Yingwei Mao − *The Huck Institutes of the Life Sciences and Department of Biology, The Pennsylvania State University, University Park, Pennsylvania 16802, United States*; Phone: 1-(814)867-4739; Email: yzm1@psu.edu

Mauricio Terrones − *Department of Physics, Material Research Institute, The Huck Institutes of the Life Sciences, Department of Chemistry, and Department of Materials Science & Engineering, The Pennsylvania State University, University Park, Pennsylvania 16802, United States*; orcid.org/0000-0003-0010-2851; Phone: 1-(814) 865-0343; Email: mut11@psu.edu

Authors

Yin-Ting Yeh − *Department of Physics, Material Research Institute, and The Huck Institutes of the Life Sciences, The Pennsylvania State University, University Park, Pennsylvania 16802, United States*; orcid.org/0000-0002-1512-9267

Yijing Zhou − *The Huck Institutes of the Life Sciences and Department of Biology, The Pennsylvania State University, University Park, Pennsylvania 16802, United States*

Donghua Zou − *Department of Neurology, The Fifth Affiliated Hospital of Guangxi Medical University, Nanning, Guangxi 530022, China*

He Liu − *Department of Chemistry, The Pennsylvania State University, University Park, Pennsylvania 16802, United States*

Haiyang Yu − *Department of Veterinary and Biomedical Science, The Pennsylvania State University, University Park, Pennsylvania 16802, United States*

Huaguang Lu − *Department of Veterinary and Biomedical Science, The Pennsylvania State University, University Park, Pennsylvania 16802, United States*

Venkataraman Swaminathan − *Department of Physics, The Pennsylvania State University, University Park, Pennsylvania 16802, United States*

Complete contact information is available at: https://pubs.acs.org/10.1021/acsami.9b20990

Author Contributions

Y.-T.Y. designed, conducted the experiments, and composed the manuscript. Y.Z. conducted the experiments and edited the manuscript. D.Z. conducted the experiments. H.L. prepared nanomaterials for the experiments. H.Y. conducted the cell-related experiments. V.S. reviewed and edited the manuscript. Y.M. designed, reviewed the manuscript, and guided the project. M.T. designed the experiment and guided the project.

Notes

The authors declare no competing financial interest.

■ ACKNOWLEDGMENTS

The authors thank the National Science Foundation Growing Convergence Research Big Idea under grant no. 1934977, the Thrasher Research Fund (TRF13731), the Infectious Disease Research Exchanges Grant from Princeton University, and the start-up fund (402854 UP1001 ST-YEH) from the Pennsylvania State University. This project was supported by Thrasher Research Fund (TRF13731), United States Department of Agriculture (USDA Nanotube 404-49 75W3), Infectious Disease Research Exchanges Grant from Princeton University, and the start-up fund (402854 UP1001 ST-YEH) from the Pennsylvania State University.

■ REFERENCES

(1) Colombo, M.; Raposo, G.; Théry, C. Biogenesis, secretion, and intercellular interactions of exosomes and other extracellular vesicles. *Annu. Rev. Cell Dev. Biol.* **2014**, *30*, 255−289.

(2) Gould, S. J.; Raposo, G. As we wait: coping with an imperfect nomenclature for extracellular vesicles. *J. Extracell. Vesicles* **2013**, *2*, 20389.

(3) Johnstone, R. M.; Adam, M.; Hammond, J. R.; Orr, L.; Turbide, C. Vesicle formation during reticulocyte maturation. Association of plasma membrane activities with released vesicles (exosomes). *J. Biol. Chem.* **1987**, *262*, 9412−9420.

(4) van Niel, G.; D'Angelo, G.; Raposo, G. Shedding light on the cell biology of extracellular vesicles. *Nat. Rev. Mol. Cell Biol.* **2018**, *19*, 213−228.

(5) Okoye, I. S.; Coomes, S. M.; Pelly, V. S.; Czieso, S.; Papayannopoulos, V.; Tolmachova, T.; Seabra, M. C.; Wilson, M. S. MicroRNA-Containing T-Regulatory-Cell-Derived Exosomes Suppress Pathogenic T Helper 1 Cells. *Immunity* **2014**, *41*, 503.

(6) Montecalvo, A.; Larregina, A. T.; Shufesky, W. J.; Beer Stolz, D.; Sullivan, M. L. G.; Karlsson, J. M.; Baty, C. J.; Gibson, G. A.; Erdos, G.; Wang, Z.; Milosevic, J.; Tkacheva, O. A.; Divito, S. J.; Jordan, R.; Lyons-Weiler, J.; Watkins, S. C.; Morelli, A. E. Mechanism of transfer of functional microRNAs between mouse dendritic cells via exosomes. *Blood* **2012**, *119*, 756−766.

(7) Théry, C.; Duban, L.; Segura, E.; Véron, P.; Lantz, O.; Amigorena, S. Indirect activation of naive CD4+ T cells by dendritic cell-derived exosomes. *Nat. Immunol.* **2002**, *3*, 1156−1162.

(8) Syn, N. L.; Wang, L.; Chow, E. K.-H.; Lim, C. T.; Goh, B.-C. Exosomes in Cancer Nanomedicine and Immunotherapy: Prospects and Challenges. *Trends Biotechnol.* **2017**, *35*, 665−676.

(9) Yamamoto, S.; Azuma, E.; Muramatsu, M.; Hamashima, T.; Ishii, Y.; Sasahara, M. Significance of Extracellular Vesicles: Pathobiological Roles in Disease. *Cell Struct. Funct.* **2016**, *41*, 137−143.

(10) Rajendran, L.; Bali, J.; Barr, M. M.; Court, F. A.; Kramer-Albers, E.-M.; Picou, F.; Raposo, G.; van der Vos, K. E.; van Niel, G.; Wang, J.; Breakefield, X. O. Emerging roles of extracellular vesicles in the nervous system. *J. Neurosci.* **2014**, *34*, 15482−15489.

(11) Zhang, Y.; Wang, Q.; Wang, H.; Duan, E. Uterine Fluid in Pregnancy: A Biological and Clinical Outlook. *Trends Mol. Med.* **2017**, *23*, 604−614.

(12) Karpman, D.; Ståhl, A.-l.; Arvidsson, I. Extracellular vesicles in renal disease. *Nat. Rev. Nephrol.* **2017**, *13*, 545−562.

(13) Raab-Traub, N.; Dittmer, D. P. Viral effects on the content and function of extracellular vesicles. *Nat. Rev. Microbiol.* **2017**, *15*, 559−572.
(14) Hall, J.; Prabhakar, S.; Balaj, L.; Lai, C. P.; Cerione, R. A.; Breakefield, X. O. Delivery of Therapeutic Proteins via Extracellular Vesicles: Review and Potential Treatments for Parkinson's Disease, Glioma, and Schwannoma. *Cell. Mol. Neurobiol.* **2016**, *36*, 417−427.
(15) Frühbeis, C.; Frohlich, D.; Kuo, W. P.; Kramer-Albers, E. M. Extracellular vesicles as mediators of neuron-glia communication. *Front. Cell. Neurosci.* **2013**, *7*, 182.
(16) Liu, S.; Hossinger, A.; Göbbels, S.; Vorberg, I. M. Prions on the run: How extracellular vesicles serve as delivery vehicles for self-templating protein aggregates. *Prion* **2017**, *11*, 98−112.
(17) Van Giau, V.; An, S. S. A. Emergence of exosomal miRNAs as a diagnostic biomarker for Alzheimer's disease. *J. Neurol. Sci.* **2016**, *360*, 141−152.
(18) Merchant, M. L.; Rood, I. M.; Deegens, J. K. J.; Klein, J. B. Isolation and characterization of urinary extracellular vesicles: implications for biomarker discovery. *Nat. Rev. Nephrol.* **2017**, *13*, 731−749.
(19) Ferrara, D.; Pasetto, L.; Bonetto, V.; Basso, M. Role of Extracellular Vesicles in Amyotrophic Lateral Sclerosis. *Front. Neurosci.* **2018**, *12*, 574.
(20) Coumans, F. A. W.; Brisson, A. R.; Buzas, E. I.; Dignat-George, F.; Drees, E. E. E.; El-Andaloussi, S.; Emanueli, C.; Gasecka, A.; Hendrix, A.; Hill, A. F.; Lacroix, R.; Lee, Y.; van Leeuwen, T. G.; Mackman, N.; Mäger, I.; Nolan, J. P.; van der Pol, E.; Pegtel, D. M.; Sahoo, S.; Siljander, P. R. M.; Sturk, G.; de Wever, O.; Nieuwland, R. Methodological Guidelines to Study Extracellular Vesicles. *Circ. Res.* **2017**, *120*, 1632−1648.
(21) Andaloussi, S. E.; Mager, I.; Breakefield, X. O.; Wood, M. J. Extracellular vesicles: biology and emerging therapeutic opportunities. *Nat. Rev. Drug Discov.* **2013**, *12*, 347−357.
(22) Leiblich, A. Recent Developments in the Search for Urinary Biomarkers in Bladder Cancer. *Curr. Urol. Rep.* **2017**, *18*, 100.
(23) Li, P.; Kaslan, M.; Lee, S. H.; Yao, J.; Gao, Z. Progress in Exosome Isolation Techniques. *Theranostics* **2017**, *7*, 789−804.
(24) van der Pol, E.; Böing, A. N.; Gool, E. L.; Nieuwland, R. Recent developments in the nomenclature, presence, isolation, detection and clinical impact of extracellular vesicles. *J. Thromb. Haemostasis* **2016**, *14*, 48−56.
(25) Liga, A.; Vliegenthart, A. D. B.; Oosthuyzen, W.; Dear, J. W.; Kersaudy-Kerhoas, M. Exosome isolation: a microfluidic road-map. *Lab Chip* **2015**, *15*, 2388−2394.
(26) Terrones, M. Science and Technology of the Twenty-First Century: Synthesis, Properties, and Applications of Carbon Nanotubes. *Annu. Rev. Mater. Res.* **2003**, *33*, 419−501.
(27) Yu, L.; Shearer, C.; Shapter, J. Recent Development of Carbon Nanotube Transparent Conductive Films. *Chem. Rev.* **2016**, *116*, 13413−13453.
(28) Lu, F.; Gu, L.; Meziani, M. J.; Wang, X.; Luo, P. G.; Veca, L. M.; Cao, L.; Sun, Y.-P. Advances in Bioapplications of Carbon Nanotubes. *Adv. Mater.* **2009**, *21*, 139−152.
(29) Yeh, Y.-T.; Lin, Z.; Zheng, S. Y.; Terrones, M. A carbon nanotube integrated microfluidic device for blood plasma extraction. *Sci. Rep.* **2018**, *8*, 13623.
(30) Yeh, Y.-T.; Tang, Y.; Sebastian, A.; Dasgupta, A.; Perea-Lopez, N.; Albert, I.; Lu, H.; Terrones, M.; Zheng, S.-Y. Tunable and label-free virus enrichment for ultrasensitive virus detection using carbon nanotube arrays. *Sci. Adv.* **2016**, *2*, No. e1601026.
(31) Yeh, Y. T.; Tang, Y.; Lu, H.; Terrones, M.; Zheng, S. Y. A Vacnt Integrated Handheld Device For Label-Free Virus Capture, Detection And Enrichment For Genomic Analysis. *2015 Transducers—2015 18th International Conference on Solid-State Sensors, Actuators and Microsystems (TRANSDUCERS)*; IEEE, 2015; pp 747−750.
(32) Yeh, Y. T.; Perea-Lopez, N.; Dasgupta, A.; Harouaka, R.; Terrones, M.; Zheng, S. Y. Microfluidic Device With Carbon Nanotube Channel Walls For Blood Plasma Extraction. *2013 IEEE 26th International Conference on Micro Electro Mechanical Systems (MEMS)*; IEEE, 2013; pp 951−954.
(33) Elías, A. L.; Carrero-Sánchez, J. C.; Terrones, H.; Endo, M.; Laclette, J. P.; Terrones, M. Viability studies of pure carbon- and nitrogen-doped nanotubes with Entamoeba histolytica: from amoebicidal to biocompatible structures. *Small* **2007**, *3*, 1723−1729.
(34) Carrero-Sánchez, J. C.; Elías, A. L.; Mancilla, R.; Arrellín, G.; Terrones, H.; Laclette, J. P.; Terrones, M. Biocompatibility and toxicological studies of carbon nanotubes doped with nitrogen. *Nano Lett.* **2006**, *6*, 1609−1616.
(35) Yeh, Y.-T.; Gulino, K.; Zhang, Y.; Sabestien, A.; Chou, T.-W.; Zhou, B.; Lin, Z.; Albert, I.; Lu, H.; Swaminathan, V.; Ghedin, E.; Terrones, M. A rapid and label-free platform for virus capture and identification from clinical samples. *Proceedings of the National Academy of Sciences*, 2020.
(36) Yeh, Y. T.; Tang, Y.; Lu, H.; Terrones, M.; Zheng, S. Y. A VACNT integrated handheld device for label-free virus capture, detection and enrichment for genomic analysis. *2015 Transducers—2015 18th International Conference on Solid-State Sensors, Actuators and Microsystems (TRANSDUCERS), 21−25 June 2015*, 2015; pp 747−750.
(37) Stott, S. L.; Hsu, C.-H.; Tsukrov, D. I.; Yu, M.; Miyamoto, D. T.; Waltman, B. A.; Rothenberg, S. M.; Shah, A. M.; Smas, M. E.; Korir, G. K.; Floyd, F. P.; Gilman, A. J.; Lord, J. B.; Winokur, D.; Springer, S.; Irimia, D.; Nagrath, S.; Sequist, L. V.; Lee, R. J.; Isselbacher, K. J.; Maheswaran, S.; Haber, D. A.; Toner, M. Isolation of circulating tumor cells using a microvortex-generating herringbone-chip. *Proc. Natl. Acad. Sci. U.S.A.* **2010**, *107*, 18392−18397.
(38) Stroock, A. D.; Dertinger, S. K. W.; Ajdari, A.; Mezic, I.; Stone, H. A.; Whitesides, G. M. Chaotic mixer for microchannels. *Science* **2002**, *295*, 647−651.
(39) Quek, C.; Hill, A. F. The role of extracellular vesicles in neurodegenerative diseases. *Biochem. Biophys. Res. Commun.* **2017**, *483*, 1178−1186.
(40) Morton, M. C.; Feliciano, D. M. Neurovesicles in Brain Development. *Cell. Mol. Neurobiol.* **2016**, *36*, 409−416.
(41) Krämer-Albers, E.-M.; Hill, A. F. Extracellular vesicles: interneural shuttles of complex messages. *Curr. Opin. Neurobiol.* **2016**, *39*, 101−107.
(42) Yeh, Y.-T.; Tang, Y.; Sebastian, A.; Dasgupta, A.; Perea-Lopez, N.; Albert, I.; Lu, H.; Terrones, M.; Zheng, S.-Y. Tunable and label-free virus enrichment for ultrasensitive virus detection using carbon nanotube arrays. *Sci. Adv.* **2016**, *2*, No. e1601026.
(43) Albanese, A.; Tang, P. S.; Chan, W. C. W. The Effect of Nanoparticle Size, Shape, and Surface Chemistry on Biological Systems. In *Annual Review of Biomedical Engineering, Vol 14*; Yarmush, M. L., Ed.; Annual Reviews; Palo Alto, 2012; Vol. *14*, pp 1−16.
(44) Heusermann, W.; Hean, J.; Trojer, D.; Steib, E.; von Bueren, S.; Graff-Meyer, A.; Genoud, C.; Martin, K.; Pizzato, N.; Voshol, J.; Morrissey, D. V.; Andaloussi, S. E. L.; Wood, M. J.; Meisner-Kober, N. C. Exosomes surf on filopodia to enter cells at endocytic hot spots, traffic within endosomes, and are targeted to the ER. *J. Cell Biol.* **2016**, *213*, 173−184.
(45) Thayanithy, V.; Babatunde, V.; Dickson, E. L.; Wong, P.; Oh, S.; Ke, X.; Barlas, A.; Fujisawa, S.; Romin, Y.; Moreira, A. L.; Downey, R. J.; Steer, C. J.; Subramanian, S.; Manova-Todorova, K.; Moore, M. A. S.; Lou, E. Tumor exosomes induce tunneling nanotubes in lipid raft-enriched regions of human mesothelioma cells. *Exp. Cell Res.* **2014**, *323*, 178−188.
(46) Friedman, J. R.; DiBenedetto, J. R.; West, M.; Rowland, A. A.; Voeltz, G. K.; Hegde, R. S. Endoplasmic reticulum−endosome contact increases as endosomes traffic and mature. *Mol. Biol. Cell* **2013**, *24*, 1030−1040.

https://dx.doi.org/10.1021/acsami.9b20990
ACS Appl. Mater. Interfaces 2020, 12, 13134−13139